ADVANCED FUNCTIONAL MATERIALS
www.afm-journal.de

Hexyl Gallate Loaded Microgels Enable Efficient Protection Against Citrus Canker

Susanne Braun, Guilherme Dilarri, Leticia C. de Lencastre Novaes, Philipp Huth, Alexander Töpel, Larissa Hussmann, Alexander Boes, Miguel Divino da Rocha, Felix Jakob, Luis Octavio Regasini, Ulrich Schwaneberg, Henrique Ferreira,* and Andrij Pich**

The development of efficient and environmentally friendly plant protection systems is one of the major challenges for a sustainable agriculture of the future. Citrus canker caused by the pathogen *Xanthomonas citri* subsp. *citri* (*X. citri*) affects all cultivated citrus species worldwide and is responsible for enormous economic losses and restrictions in international trade. Currently used commercial copper-based formulations are the origin of contamination for soil and groundwater, affecting local ecosystems and human health. A copper-free sustainable microgel-based plant protection system able to efficiently combat *X. citri* is developed. Microgels decorated with anchor peptides exhibit strong non-covalent attachment to the surface of orange leaves and have the ability to release hexyl gallate, which inhibits the growth and spreading of pathogens. The tailored design of the microgel network allows high loadings of hexyl gallate (up to 40 wt.%) and a controlled release of gallates from microgels that provide long-term protection. The antibacterial activity of the hexyl gallate-loaded microgels is demonstrated by various in vitro assays as well as on orange plants in greenhouse settings. The experimental results suggest that the developed sustainable microgel-based plant protection system for citrus trees allows efficient abatement of *X. citri* and reduces environmental pollution caused by copper formulations.

1. Introduction

Citrus plants originated in tropical and subtropical Southeast Asia, and citrus fruits are known to be rich in bioactive compounds and vitamin C, and are considered a rich source of nutrients for the human body.[1] According to the latest survey by the Food and Agriculture Organization of the United Nations (FAOSTAT), the three largest citrus producers in the world are China, Brazil, and India, respectively.[2] Brazil is the world leader in sweet orange production and the biggest exporter of orange juice in an economic activity that generates thousands of jobs and ≈2 billion dollars/year of income revenue.[3,4] However, concerns for the citrus-producing countries include the diseases that affect citrus cultivars causing great losses for the orange juice industry. Bacterial diseases, in particular, represent constant threats to citriculture, being Huanglongbing (HLB) and citrus canker the main ones and they are responsible for significant reductions in citrus production.[5,6]

S. Braun, L. C. de Lencastre Novaes, P. Huth, A. Töpel, L. Hussmann, A. Boes, F. Jakob, U. Schwaneberg, A. Pich
DWI – Leibniz Institute for Interactive Materials e. V.
Forckenbeckstr. 50, 52074 Aachen, Germany
E-mail: u.schwaneberg@biotec.rwth-aachen.de; pich@dwi.rwth-aachen.de

S. Braun, P. Huth, A. Töpel, L. Hussmann, A. Pich
Functional and Interactive Polymers
Institute of Technical and Macromolecular Chemistry (ITMC)
Worringerweg 2, 52074 Aachen, Germany

G. Dilarri, H. Ferreira
Institute of Biosciences
Biochemistry Building
State University of Sao Paulo
Avenida 24-A 1515, Rio Claro, SP 13506-900, Brazil
E-mail: henrique.ferreira@unesp.br

G. Dilarri
Department of Fisheries Engineering and Biological Sciences
Santa Catarina State University (UDESC)
Rua Coronel Fernandes Martins 270, Laguna, SC 88790-000, Brazil

M. D. da Rocha, L. O. Regasini
Institute of Biosciences
Humanities and Exact Sciences
State University of Sao Paulo
Rua Cristóvão Colombo 2265, São José do Rio Preto, SP 15054-000, Brazil

U. Schwaneberg
Institute of Biotechnology
RWTH Aachen University
Worringerweg 3, 52056 Aachen, Germany

A. Pich
Aachen Maastricht Institute for Biobased Materials (AMIBM)
Maastricht University Brightlands Chemelot Campus
Urmonderbaan 22, Geleen 6167 RD, Netherlands

The ORCID identification number(s) for the author(s) of this article can be found under https://doi.org/10.1002/adfm.202305646

DOI: 10.1002/adfm.202305646

Citrus canker is caused by the Gram-negative bacterium *Xanthomonas citri* subsp. *citri (X. citri)*. The disease is spread by wind and rain, contaminating plants in the surroundings and also new and distant areas in the vicinities.[7–9] In severe cases, the infection by *X. citri* can lead to defoliation and consequently fruit drop.[7,9,10] Once the plant or fruit is infected, lesions appear in the plant tissues, characterized as cortical, circular, and salient lesions, with a yellowish or brown color and eruptive appearance.[9] In addition, the commercialization of fruits contaminated with *X. citri* is prohibited, since citrus canker is considered a quarentenary disease.[11,12]

Citrus canker is now endemic in the largest orange-producing area in Brazil, the state of São Paulo, which composes the Brazilian citrus belt. The control of the disease in this state is exerted by combined agricultural practices including recurrent sprays of copper solutions in the orchards. Copper has been used in agriculture for over 160 years in the management of plant diseases.[13] However, the massive use of copper in agriculture has raised concerns about its consequences, being some negative aspects already associated with diseases in humans, such as Alzheimer's.[14] The copper ions are generally immobile in the soil. Therefore, the continuous spraying of copper results in metal accumulation in the soil, reaching toxic levels for living organisms, and causing stress on plants. In addition, high levels of copper can impact the biodiversity of the soil/water microbiota, which can consequently reduce the soil fertility and water quality.[14–16] Copper can also accumulate throughout the food chain, contaminating and impacting many animals and plants. For these reasons, organic farmers are increasingly trying to minimize the use of copper.[17] The identification of genes able to confer resistance to copper in some *X. citri* isolates,[18] added to the negative impact of excess copper in agriculture, supports the necessity for alternatives for disease management, reducing or even replacing the application of copper in the field.

Among the possible alternatives to copper, esters of gallic acid (gallates) have been studied and applied as inhibitors of *X. citri* in vitro and in vivo under controlled conditions.[19–22] However, the gallates studied so far have insufficient water solubility for spray applications and poor foliar fixation to ensure a prolonged bacterial inhibition effect after the application, which hampers their direct application as agricultural defensives.

Microgels are colloidal 3D polymer networks, that combine properties of rigid particles and flexible macromolecules.[23–26] Stimuli-responsive microgels are able to reversibly change their swelling degree in response to environmental stimuli, such as changes in temperature,[27] pH,[28] light,[29] ionic strength,[30] or mechanical force.[31,32] The porous internal structure, small size, and colloidal stability in aqueous solutions render microgels perfect candidates as carriers for the delivery of active molecules. The molecular engineering of the microgel interior allows integration of charges[33,34] or hydrophobic domains[35,36] to ensure the loading of drugs,[37] peptides, or proteins.[38] The release of the payload can be controlled by pH, temperature, or degradation of cross-links.[37,39]

Recently, we demonstrated that microgels decorated with anchor peptides exhibit strong and selective binding to leaves of cucumber plants.[40] Anchor peptides are adhesion-promoting peptides, with sizes ranging from 20–100 amino acids, and enable surface functionalization at room temperature using a water-based solution.[40–42] The anchor-peptide concept is based on natural antimicrobial peptides, which interact with biological membranes, due to their amphipathic structure,[43] considered essential for their binding and insertion into microbial membranes.[44] It has been shown that microgels decorated by anchor peptides can serve as carriers for the delivery of micronutrients to Fe^{3+}-deficient plants.[40]

In terms of sustainable crop protection, three major areas converge: i) mechanical protection measures, ii) biological, and iii) chemical technologies.[45] Biological technologies include methods to make plants genetically more resistant to pathogens and thus reduce the use of additional pesticides,[46] as well as identifying natural enemies and competitors.[45] The goal of chemical crop protection is to produce insecticides, pesticides, fungicides, and herbicides.[45] For some time, however, more sustainable concepts have increasingly come into focus. In this context, natural products have played an important role in the development in the past and are still a continuous source of innovation in the discovery of crop protection products.[47] One of the most innovative methods of crop protection is the development of nanosized pesticides and nanocarriers, such as the sustainably generated cellulose nanocrystals.[48]

Thus, this work aimed to synthesize and evaluate the potential of hexyl gallate (G6) loaded microgels decorated with anchor peptides as an alternative to copper formulations for the protection of citrus plants against *X. citri* infection. In the present work, microgels with covalent and supramolecular cross-links were synthesized and characterized in terms of their chemical composition (quantitative Raman spectroscopy), size and size distribution (dynamic light scattering (DLS)), morphology (electron and atomic force microscopy) and surface charge (electrophoretic light scattering (ELS)). In order to guarantee strong adhesion to the leaf's surface, an anchor peptide has been selected for the attachment on the wax of the orange tree leaves. The successful conjugation of the anchor peptide to microgels was investigated by fluorescence spectroscopy and confocal microscopy. The loading and the release of the antimicrobial active component G6 were investigated using quantitative ^{1}H-NMR spectroscopy. Finally, the antimicrobial activity against the *X. citri* was examined and validated using in vitro microbiological analyses, and subsequently plant protection tests in greenhouse scale.

2. Results and Discussion

The present work aimed to develop a microgel-based plant protection system for citrus plants against infection by the citrus canker causative agent *X. citri*. (**Scheme 1**). The use of microgels for the encapsulation of the hydrophobic, antimicrobial compound G6 enables the use of aqueous dispersions for application onto plants in the orchards.

As shown in Scheme 1, we selected two types of microgels for this study: covalently cross-linked, non-degradable microgels and physically cross-linked, pH-degradable microgels. We hypothesize that the nature of the cross-links in microgels will influence the release of active molecules and their degradability. To provide a strong binding to the leaves of orange trees, the microgels were decorated with anchor peptides, which showed the strongest binding to the wax of orange leaves. Subsequently, the microgel/anchor peptide conjugates were loaded with the

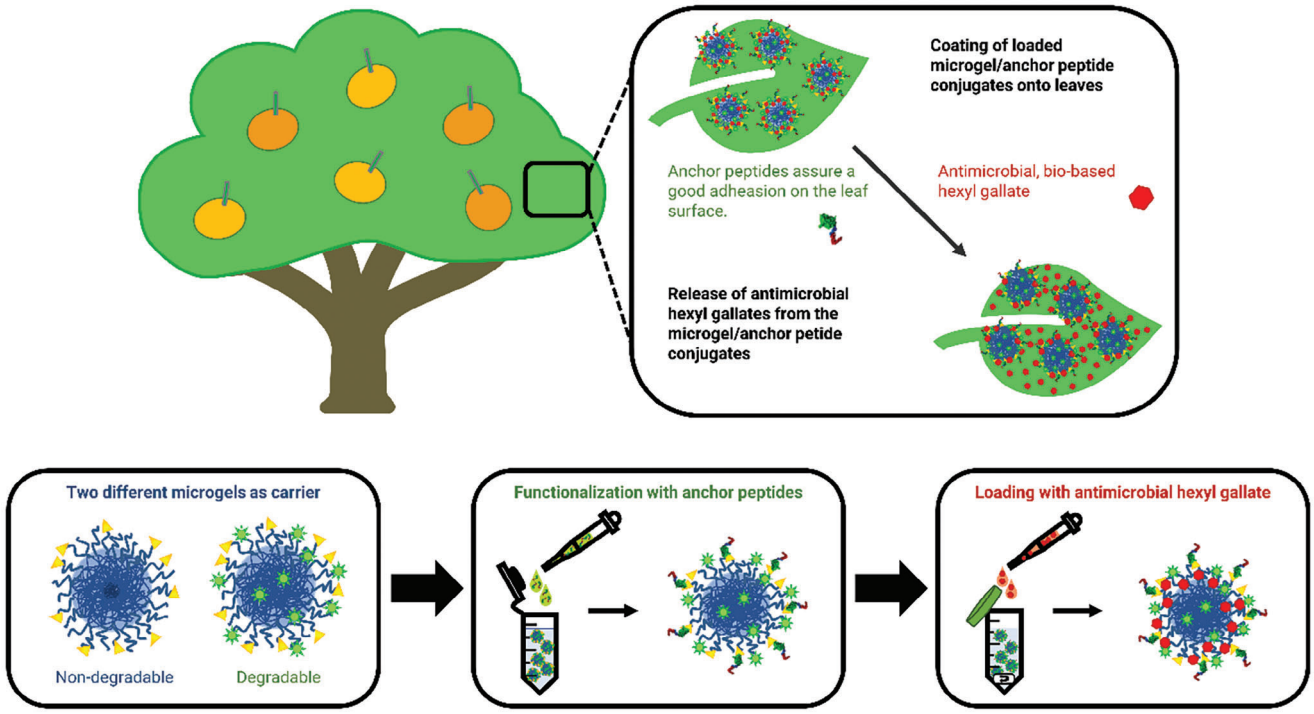

Scheme 1. Schematic illustration showing the innovative approach to protect citrus against *X. citri* using hexyl gallate-loaded microgels as substitute of environmentally harmful copper formulations.

bio-based, antimicrobial active compound G6. Applied on the orange tree they should release the G6 slowly and steadily to provide a long-term protection. The anchor peptides should enhance the binding to the leaf surface and improve the rain fastness for long-term protection, which is one of the major advantages of the encapsulation into the microgel-anchor peptide conjugates.

2.1. Synthesis and Characterization of Microgels

Poly(N-vinylcaprolactam) (pVCL)-based microgels were synthesized using free-radical precipitation polymerization in water with 2,2′-azobis(2-methylpropionamidine) dihydrochloride (V-50) as initiator (**Figure 1**a). A small amount of the comonomer glycidyl methacrylate (GMA) was used in the microgel synthesis to integrate reactive epoxy groups into the microgel structure. The addition of GMA to the polymerization mixture was performed in a semi-batch synthesis to ensure a good accessibility and localization of epoxy groups in the outer shell of the microgels.[38] These functional groups were used to bind the anchor peptide covalently to the microgels via reaction with the thiol group of the amino acid cysteine within the eGFP-anchor peptide fusion protein.

To synthesize non-degradable microgels the most widely used covalent cross-linker *N,N'*-methylenebisacrylamide (BIS) was used. To synthesize physically cross-linked, degradable microgels the nature-derived polyphenol tannic acid (TA) was selected. The polymerization routes to synthesize microgels used in this study are shown in Figure 1a.

To ensure that the epoxide ring of GMA is not undergoing an acid catalyzed ring opening due to the presence of TA during the microgel synthesis, ^{1}H NMR stability tests were performed at 25 °C (room temperature) and 70 °C (polymerization temperature) (Figure S1, Supporting Information). Following the signals at a chemical shift of 3.44 ppm, indicating an intact epoxide ring, in all ^{1}H-NMR spectra, it is concluded that the presence of TA is not causing significant ring opening of the epoxide moiety at a reaction temperature of 70 °C.

The chemical composition of the microgels was characterized by Raman spectroscopy (Figure S2, Supporting Information). The characteristic signals of the VCL units correspond to the C-H vibrations at a wavenumber of 2930 cm^{-1} and the C═O vibrations at a wavenumber of 1625 cm^{-1}. The characteristic signal of the GMA units can be found at a wavenumber of 1729 cm^{-1} that corresponds to the C═O group. For TA, however, the characteristic signals are located in a similar range at 1711 cm^{-1} for the C═O groups and at a wavenumber of 1615 cm^{-1} for C─C and C═C bonds. Figure 1b presents the quantitative contents of key components in microgels indicating that the experimentally determined values are in good agreement with the expected ones. The calibration curve to determine GMA contents in pVCL microgels was taken from the literature.[38] The calibration curve for the quantification of the TA content is given in Figure S3 (Supporting Information). Higher GMA contents in microgels can be explained by incomplete VCL conversion and loss of non-cross-linked pVCL chains during the dialysis step. DLS data presented in Figure 1c indicate that BIS-cross-linked microgels are larger compared to TA-cross-linked ones that can be explained by the

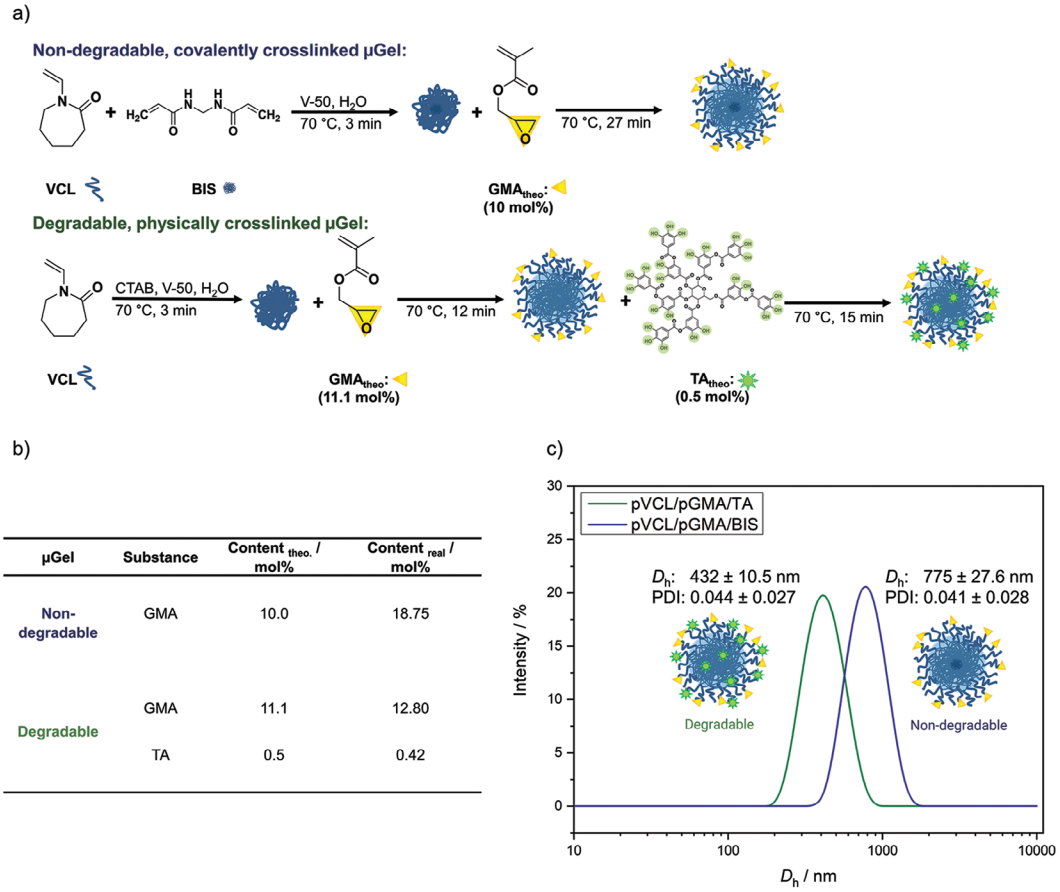

µGel	Substance	Content theo. / mol%	Content real / mol%
Non-degradable	GMA	10.0	18.75
Degradable	GMA	11.1	12.80
	TA	0.5	0.42

Figure 1. Microgel synthesis and characterization; a) reaction scheme of the semi-batch precipitation polymerization of covalently cross-linked pVCL/pGMA/BIS-, and physically cross-linked pVCL/pGMA/TA-microgels, b) quantified contents of comonomer GMA and cross-linker TA obtained by Raman spectroscopy, and c) size distribution curves obtained by DLS measurements at a scattering angle of 174.7°, $N = 3$.

use of small amounts of surfactant for the latter one as well as by the stabilizing ability of TA molecules (Figure S4, Supporting Information). The synthesized microgels exhibit temperature responsiveness reflected in the reversible change of the swelling degree as a function of the temperature (Figure S5, Supporting Information). DLS measurements performed in the temperature range of 20–60 °C indicate that both microgel types exhibit a volume phase transition temperature (VPTT) ≈34 °C, which is a characteristic property of pVCL-based microgels[49] (Figure S6, Supporting Information). The TA-cross-linked microgel exhibits a strong negative charge as determined by ELS (Figure S7, Supporting Information). Both microgel samples exhibit excellent colloidal stabilities due to the combination of steric and electrostatic stabilization. The pH-induced degradation of pVCL-based microgels cross-linked with TA has been demonstrated several times in the literature.[39] In the case of pVCL/pGMA/TA microgels, simply increasing the pH to strongly alkaline conditions failed to detect the degradation as long as an aqueous system was measured using DLS. This is likely due to the hydrophobic comonomer GMA stabilizing the polymer network by formation of physical cross-links. Nevertheless, a small increase in size and PDI is observed (Figure S8, Supporting Information). Upon dispersion in DMSO, the size as well as the PDI of microgels increase significantly. In addition, a second small peak is observed, indicating degradation. When the microgels are first dispersed in alkaline medium and the dispersion is then dispersed in DMSO, degradation is clearly observed (Figure S8, Supporting Information). Under alkaline conditions TA is deprotonated and thus the microgel network is no longer cross-linked. GMA dissolves well in DMSO, therefore this medium is suitable to show that the microgel degradation is taking place.

2.2. Selection of Anchor Peptides

The negative control eGFP and five selected anchor peptides Macaque histatin (MacHis), LCI, Plantaricin A, hDermcidin (hDerm), and Spinigerin fused to eGFP were used to test their ability to bind to the surface of orange leaves, through the analysis of the fluorescent signal of the eGPF using confocal fluorescent microscopy (**Figure 2**). In these experiments, we focused on the abaxial side of the leaves, one of the main entry points of *X. citri* is through the stomata. MacHis did not bind to the orange leaves, while LCI, Plantaricin A and Spinigerin showed a weak binding to the leaves. The anchor peptide hDerm showed the strongest binding to the leaves and was therefore chosen for the microgel decoration. For the conjugation of the anchor peptide with the

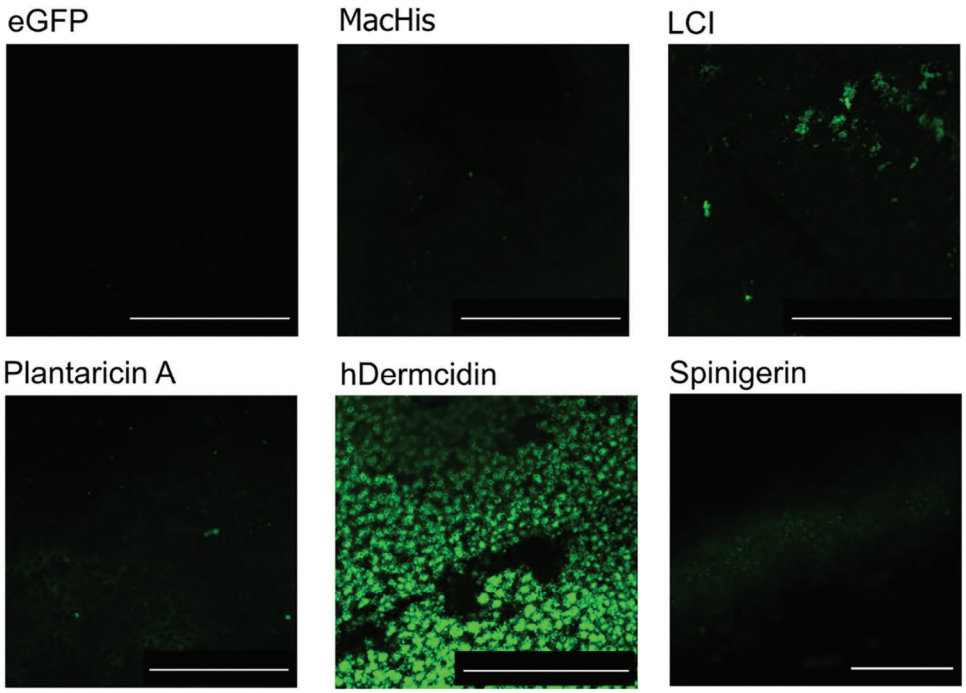

Figure 2. Confocal microscopy images of abaxial side of an orange leaf after washing the anchor peptides fused to eGFP (scale bars 500 µm).

microgel, a –SH group present on the eGFP (Cys48) is freely accessible for the conjugation with the epoxide group of the GMA moieties within the microgels structure.

2.3. Post-Functionalization and Loading of Microgels with Anchor Peptides and Antimicrobial Compound

The post-functionalization of the microgels was performed in two steps, first the decoration with the anchor peptides and then subsequently the loading with the antimicrobial active compound G6 (Figure S9, Supporting Information).

For the decoration with the anchor peptide hDerm, the microgels were dispersed in TRIS buffer (50 mM, pH 8) before the anchor peptide was added. Here, the coupling of the anchor peptide hDerm to the microgels was achieved by a click reaction between the accessible epoxide moieties of the comonomer GMA and the thiol group of the cysteine in the eGFP-anchor peptide fusion protein (Figure S9a, Supporting Information).

Laser scanning confocal microscopy (**Figure 3**a) showed that anchor peptides were grafted onto the microgels (fluorescence image). In addition, it can be confirmed that microgels do not form aggregates in aqueous dispersions (brightfield image).

Purified microgels and microgel anchor peptide conjugates were diluted to the same mass concentration and analyzed by the fluorescence signal obtained at 485 nm excitation and 520 nm emission in a microtiter plate (MTP) (Figure 3b). Here, it can be seen that pVCL/pGMA/BIS/hDerm microgels show a more intense signal (≈2-fold) than pVCL/pGMA/TA/hDerm microgels, indicating that pVCL/pGMA/BIS/hDerm microgels could bind more of the anchor peptide hDerm_eGFP. This suggests that there are maybe not as many accessible GMA groups on the surface of the pVCL/pGMA/TA microgels as there are on the surface of the pVCL/pGMA/BIS microgels. If the epoxide groups are not located on the microgels surface it is sterically difficult for the bulky eGFP anchor peptide fusion proteins to bind to the microgels. Another aspect explaining the more intense signal of pVCL/pGMA/BIS/hDerm microgel conjugates compared to pVCL/pGMA/TA/hDerm microgel conjugates could be the higher amount of incorporated GMA (Figure 1b). More conjugated anchor peptide could positively influence the binding strength of the microgel conjugates to the leaf surface.

In previous studies, it was reported that anchor peptides bind to the cuticular wax of leaves.[40,50] To evaluate the binding strength of the microgel anchor peptide conjugates, pVCL/pGMA/BIS/hDerm and pVCL/pGMA/TA/hDerm, to orange tree leaves an MTP assay was performed with wells containing orange leaf cuticular wax. Initial binding as well as binding after two washing steps with water was analyzed by the fluorescence signal of bound hDerm_eGFP obtained at 485 nm excitation and 520 nm emission (Figure S10, Supporting Information). Here, similarly to the dispersions of microgel anchor peptide conjugates (Figure 3b), the signal intensity obtained was ≈2-fold more intense for pVCL/pGMA/BIS/hDerm microgel conjugates. Normalization to the fluorescence signal of the microgel conjugates, that initially bound to the wax in the MTP assay, visualizes the relative reduction after each of the two washing steps and allows a comparison of the rain fastness for the pVCL/pGMA/BIS/hDerm- and the pVCL/pGMA/TA/hDerm microgel conjugates. During the two simulated rain events no significant difference in wash-off between pVCL/pGMA/BIS/hDerm- and pVCL/pGMA/TA/hDerm microgel conjugates was observed. Obtained results show that

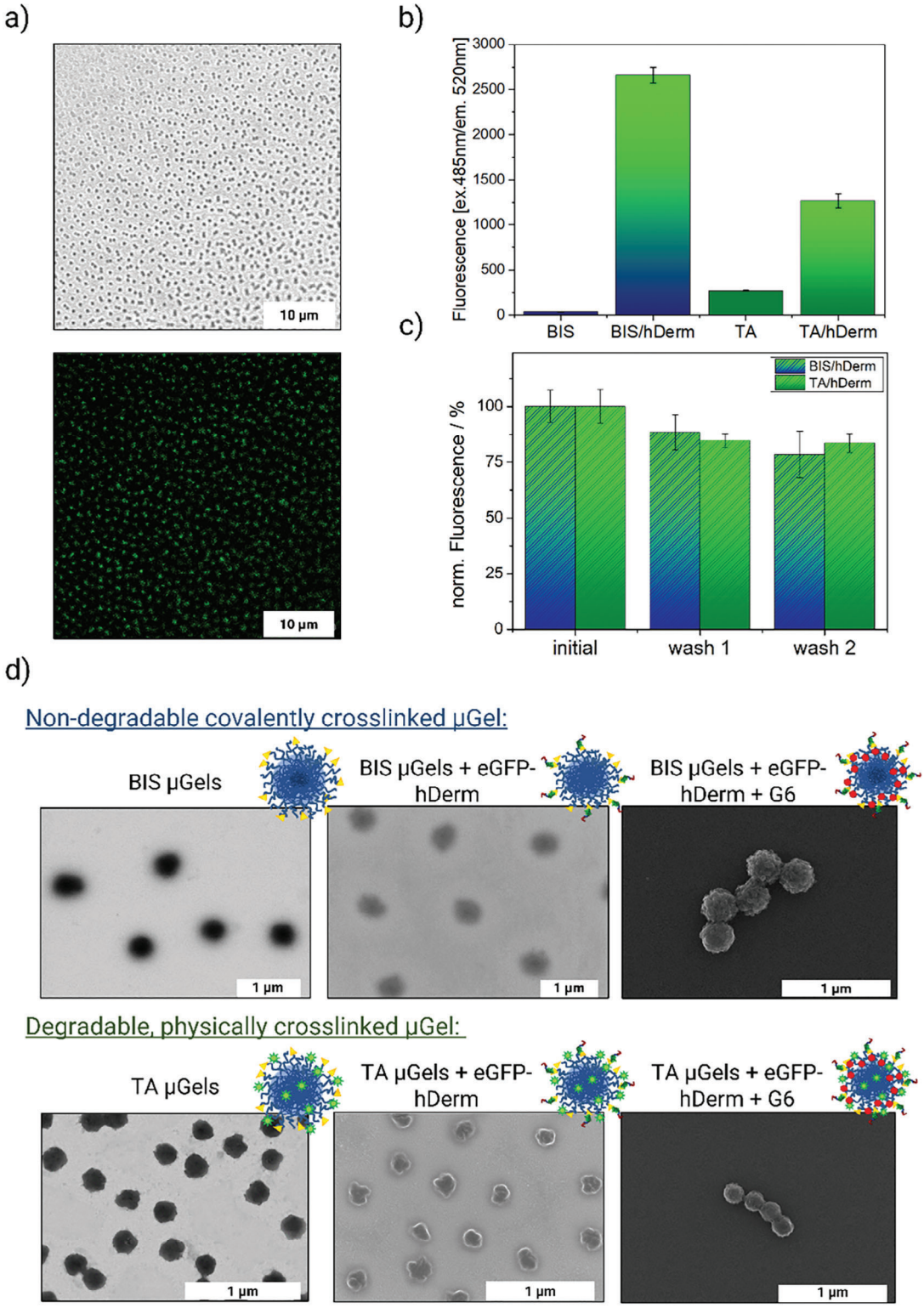

Figure 3. Characterization of microgel anchor peptide conjugates and microgel morphology before and after each step of post-functionalization: a) confocal images of pVCL/pGMA/BIS/hDerm-microgels, b) fluorescence intensity of microgel anchor peptide conjugates, $N = 3$, c) leaf binding assay of microgel anchor peptide conjugates on extracted wax from orange tree leaves showing the relative reduction by normalization to the fluorescence signal of the initially bound microgel anchor peptide conjugates and the residual fluorescence after two washing steps, $N = 3$ and d) Microgel morphology in dry state of pVCL/GMA/BIS-, pVCL/pGMA/BIS/hDerm-, pVCL/pGMA/BIS/hDerm/G6- and pVCL/GMA/TA-, pVCL/pGMA/TA/hDerm- and pVCL/pGMA/TA/hDerm/G6-microgels obtained by electron microscopy.

microgels were bound in a rain-fast manner to the cuticular wax of orange tree leaves (Figure 3c).

This technique can also be used to demonstrate the enhanced binding of microgel anchor peptide conjugates compared to undecorated microgels. Since pure pVCL/pGMA/TA microgels show an autofluorescence at an excitation wavelength of 485 and 520 nm emission (Figure 3b), which is also used to excite eGFP, they can be compared with pVCL/pGMA/TA/hDerm microgel conjugates in terms of their binding strength to orange tree leaf wax in two subsequent washing steps (Figure S11, Supporting Information). It can be seen qualitatively that the pVCL/pGMA/TA microgels also bind to the wax by themselves. However, in the normalized data (Figure S11b, Supporting Information), a faster wash-off of the undecorated microgels is observed. Based on the observed trend, it appears that the amount of anchored pVCL/pGMA/TA/hDerm microgel conjugates levels off with further washing steps, while the undecorated pVCL/pGMA/TA microgels continue to be washed off. This clearly shows that conjugation with the anchor peptide hDerm_eGFP leads to an improved rain fastness of microgels on orange tree leaf wax. For BIS cross-linked microgels, this comparison is not applicable, as no fluorescent signal is present (Figure 3b).

The loading of the microgel conjugates with the antimicrobial compound G6 was performed using the aqueous microgel dispersion. The chemical structure of G6 as well as the corresponding NMR spectra are shown in Figures S12 and S13 (Supporting Information). G6 was added and dissolved in DMSO (2.4 wt.%) in a concentration of 1 mg G6 per 1 mg of microgel. For the uptake of G6, several binding mechanisms are conceivable. On one hand, we foresee the formation of hydrogen bonds between the hydroxyl groups of the G6 and the carbonyl group of the pVCL. On the other hand, the hydrophobic interactions between lactam rings of pVCL and linear alkyl chains of G6 may take place. Also, π–π stacking of the aromatic rings present in G6s structure is possible at high loadings. We hypothesize that the combination of these molecular interactions leads to surprisingly high loadings of G6 in microgels. The stability of G6 under UV light was demonstrated by exposing G6 dissolved in DMSO-d_6 to the radiation of an LED lamp with a wavelength of 365 nm for ≈26 h. The resistance of its chemical structure was determined by NMR spectroscopy (Figure S14, Supporting Information).

The loading was at first characterized qualitatively using Raman spectroscopy (Figure S15, Supporting Information). It can be clearly seen that the signal intensity of the characteristic signals from G6 is increased drastically, suggesting a successful high loading of G6. Additionally, the G6 content was quantified via ^{1}H-NMR spectroscopy using an internal standard (Figure S16, Supporting Information). For the quantification the peak corresponding to the aromatic H-atoms of the internal standard dimethyl terephthalate (DMT) at a chemical shift of ≈8 ppm as well as the peak corresponding to the aromatic H-atoms of the antimicrobial active compound G6 at a chemical shift of ≈7 ppm have been used. Based on the integration of these two peaks the mass of the active compound m_{AcCo}, namely m_{G6}, was calculated using Equation S1 (Supporting Information). The loading degree was subsequently calculated in percent using Equation S2 (Supporting Information). For both microgel systems high loading degrees of ≈44 % were achieved (pVCL/pGMA/BIS: 43.6 % and pVCL/pGMA/TA: 44.0 %).

Furthermore, the microgels have been characterized after the synthesis and after each step of post-functionalization with DLS and ELS (Figure S17, Supporting Information). It can be seen, that for both microgel systems, the size increased slightly, and the size distribution decreased after the decoration with the anchor peptide hDerm, probably due to improved steric stabilization and better colloidal stability. The loading with the hydrophobic G6, however, caused the opposite trend. The microgel size decreased due to deswelling provoked by the loading of amphiphilic gallate molecules. At the same time, the increase in size distribution indicates the formation of microgel aggregates.

In addition to DLS and ELS measurements performed in aqueous solutions, while electron microscopy (STEM and SEM) and atomic force microscopy (AFM) were performed for characterization of microgel samples in dry state (Figure 3). It is obvious from Figure 3a (SEM and STEM images) that the microgels change their morphology, in particular after G6 loading. The microgels loaded with gallates appear more rigid and dense compared to their non-loaded analogs. This is also supported by the strong reduction of deformability of the microgels (diameter:height ratio) after gallate loading derived from the AFM measurements (Figure S19e, Supporting Information). There is barely an influence due to the decoration with anchor peptides, but after the loading with G6, the microgels exhibit a strong increase in height (and reduction of diameter:height ratio) once coated on a surface. Even though the precise values differ for the two microgels used in this study, their behavior is very similar (Figure S19, Supporting Information). The corresponding AFM images are in accordance with the results obtained by electron microscopy (Figure S18, Supporting Information).

2.4. Release of Antimicrobial Hexyl Gallate

The release of the antimicrobial active compound hexyl gallate was investigated in aqueous solutions. G6-loaded microgels were filled into dialysis tubes and dialyzed for up to 22 days against demineralized water adjusted to different pH values and at different temperatures (**Figure 4**a). The conditions were chosen to mimic the field conditions to that G6-loaded microgel carrier systems are exposed to when applied to tree leaves in orchards. Slightly acidic (pH 5) and neutral (pH 7) conditions were chosen to mimic rain at ambient temperature (25 °C). In addition, conditions of scientific interest were chosen, such as a strong acidic and alkaline pH of 3 and 9, respectively, to study the influence of the pH value, or an elevated temperature of 50 °C to assess the influence of the collapsed state of the microgels.

The release of G6 is comparable for the two different G6-loaded microgels pVCL/pGMA/BIS/hDerm/G6 and pVCL/pGMA/TA/hDerm/G6 over the duration of 175 h at pH 7 and 25 °C (Figure 4b). The release of G6 from G6-loaded microgels pVCL/pGMA/TA/hDerm/G6 was evaluated in the pH range from 3 to 9 (Figure 4c). Especially interesting with regard to the field application are the experiments at pH 5 and pH 7 (relevant pH range of rain). It can be clearly stated that an increase in pH promotes the release of G6. In the neutral pH range (pH 5 and pH 7) there is basically no significant difference detectable. At a pH of 9, a release of ≈100 % was reached after 22 days. Knowing that this pH is rather unlikely for the intended

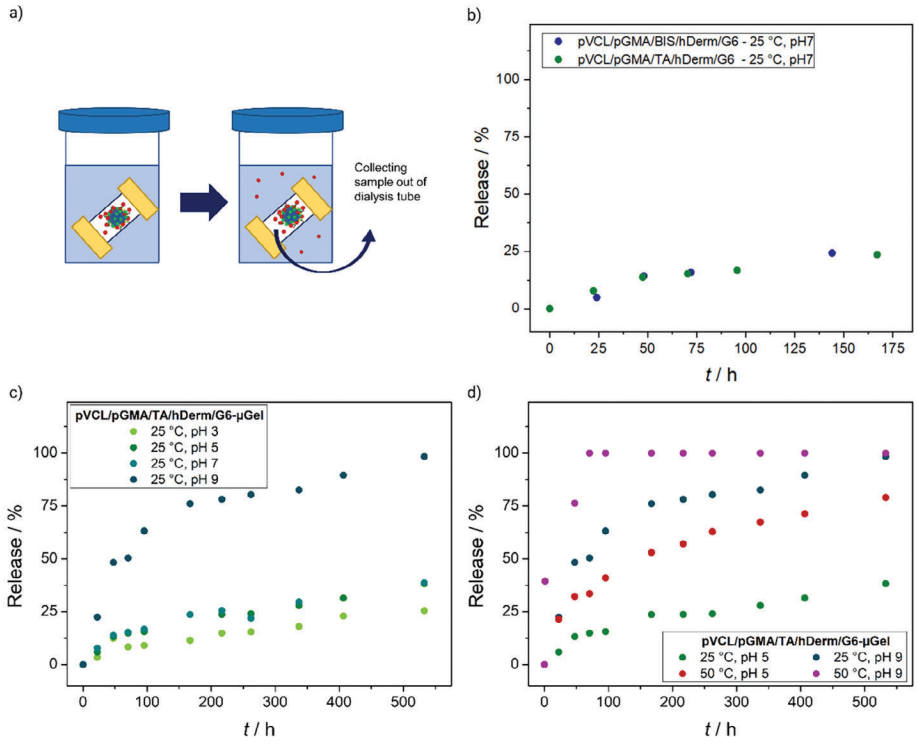

Figure 4. Release of the antimicrobial component G6 from G6-loaded microgels determined using quantitative ^{1}H-NMR spectroscopy; a) schematic illustration of the experimental setup, b) comparison of release kinetics of G6 from non-degradable pVCL/pGMA/BIS/hDerm/G6-microgels and pH-degradable pVCL/pGMA/TA/hDerm/G6-microgels for 4 days at mild conditions (pH 7 and 25 °C), c) release of G6 from pVCL/pGMA/TA/hDerm/G6-microgels as a function of pH at 25 °C and d) release of G6 from pVCL/pGMA/TA/hDerm/G6-microgels as a function of temperature and pH.

application, it still shows that a complete release of the antimicrobial active compound is possible. However, more important is that in the relevant pH range of 5–7 only 25 % of G6 are released after 22 days indicating the possibility of long-term protection of plants.

The influence of temperature on the release kinetics of G6 from the G6-loaded microgels pVCL/pGMA/TA/hDerm/G6 is shown in Figure 4c. Generally, it can be stated that the microgels are in their swollen form at 25 °C. At 50 °C, however, they are in their collapsed form. An increase in temperature promotes the G6 release from the G6-loaded microgels. At a pH of 5, the release was increased from 38 % at 25 °C to 79 % at 50 °C after 22 days. For a pH of 9 a release of 100 % is reached after 22 days at 25 °C and after only 3 days at a temperature of 50 °C. These experimental results indicate that at higher temperatures and high humidity, which typically promote bacterial growth, more antibacterial agents can be released due to temperature-responsiveness of microgels providing intrinsic self-regulation function for the plant protection system.

The release of G6 from G6-loaded, non-degradable, covalently cross-linked pVCL/pGMA/BIS/hDerm/G6-microgels, was examined at mild conditions (pH 7 and 25 °C) for 6 days (Figure S20, Supporting Information).

The release of G6 from pVCL/pGMA/TA/hDerm/G6 microgels was also tested in the presence of salt to assess the influence of saline solutions used in the in vitro antimicrobial assays. For these experiments an isotonic salt concentration was chosen at neutral pH and room temperature. The presence of salt generally promotes the release of G6 from the microgels during the first 2 days. Thereafter, the release follows the same continuous profile as in the experiment without salt (Figure S21, Supporting Information). This indicates that the presence of salt leads to a burst release in the first 2 days releasing ≈51 % of G6 from the microgels instead of ≈14 % without salt.

2.5. Bacterial Growth Inhibition

In order to verify the presence of G6 as the source of the antimicrobial activity of the G6-loaded microgel conjugates, in vitro assays were performed. In this context, both the pure microgel carrier systems and the microgel carrier systems decorated with anchor peptides were examined to identify possible contributions of the other components of the G6-loaded microgel carrier systems (**Figure 5**). In addition, the pure components, i.e. the cross-linker TA and the used anchor peptide hDerm_eGFP, were tested for their antimicrobial activity against *X. citri* (Figure S22, Supporting Information).

Two different in vitro tests, the resazurin microtiter assay (REMA) and the minimum bactericidal concentration (MBC) test, were combined to provide a robust indication of antimicrobial activity. Through monitoring bacterial respiration using the REMA assay, it was possible to evaluate the growth inhibitory activity of the microgels at different

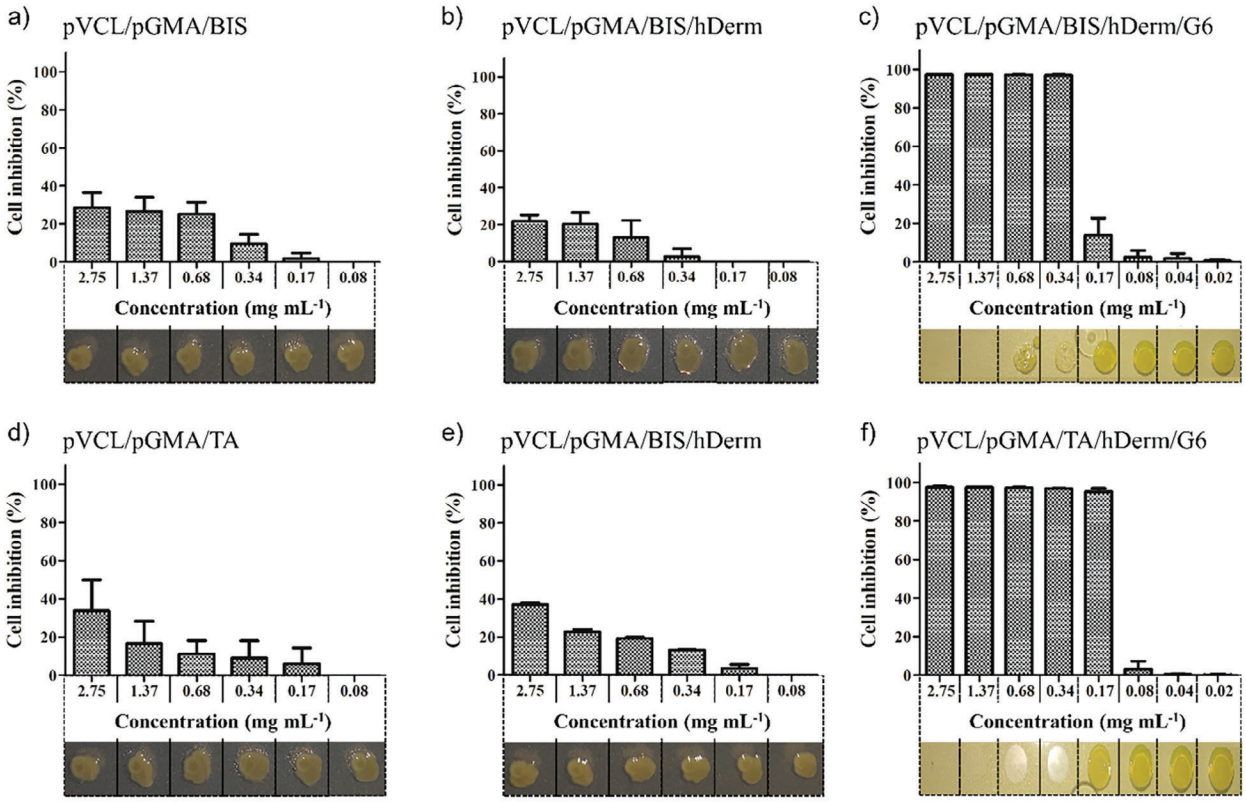

Figure 5. G6-loaded microgels inhibit *X. citri* growth in vitro. Bacterial respiration was measured by using the resazurin test (REMA) after 16 h of microgel exposure. The average percentages of cells inhibited by the microgels are represented as bars and the standard deviation of the means by the vertical lines above the bars. The minimal bactericidal concentration test (MBC) is shown underneath the graphs. a) pVCL/pGMA/BIS, b) pVCL/pGMA/BIS/hDerm, c) pVCL/pGMA/BIS/hDerm/G6, d) pVCL/pGMA/TA, e) pVCL/pGMA/TA/hDerm, and f) pVCL/pGMA/TA/hDerm/G6.

concentrations against *X. citri* cells. The results confirmed that only the G6-loaded microgels, pVCL/pGMA/BIS/hDerm/G6 and pVCL/pGMA/TA/hDerm/G6, showed inhibitory activities against *X. citri*, with IC_{100} values of 0.33 and 0.17 mg mL^{-1}, respectively (Figure 5c,f). Following the exposure to the microgels in REMA, aliquots of cell suspension were inoculated onto NYG medium (without any added compound) in order to evaluate if the microgels had bacteriostatic or bactericidal action (MBC test). As a result, *X. citri* cells were able to resume growth after treatment with both G6-loaded microgels at their IC_{100} values; therefore, these microgels exhibited only bacteriostatic action when used at their IC_{100} (Figure 5). However, the G6-loaded microgels, pVCL/pGMA/BIS/hDerm/G6 and pVCL/pGMA/TA/hDerm/G6, exhibited bactericidal action when used at the higher concentrations of 1.375 and 0.343 mg mL^{-1}, respectively (Figure 5). The microgels that did not carry any gallate exhibited the lowest growth inhibition values against *X. citri*, reaching inhibition levels between ≈30 % and 35 %.

Some anchor peptides, such as hDerm, may exhibit antibacterial effects, or they can even functionalize other reactions, which can be referred to as multifunctional peptides.[51–53] However, when tested alone against *X. citri* cells, at the highest concentration of 200 μg mL^{-1}, hDerm did not show any antimicrobial effect against this plant pathogen (Figure S22, Supporting Information).

Tannic acid (TA) has already been described as an efficient organic agent in the inhibition of a wide variety of bacteria,[54] being effective against pathogens of clinical interest such as *Staphylococcus aureus*,[55] and *Penicillium digitatum*, which is an important phytopathogen of citrus.[56] However, the incorporation of TA in some of the microgels synthesized in the present work was aimed only to cross-link the polymer network,[57,58] with no focus on its possible bactericidal action against *X. citri*. It is noteworthy that the microgels pVCL/pGMA/TA and pVCL/pGMA/TA/hDerm at the concentration of 2.75 mg mL^{-1} showed growth inhibition values of 33.67 % and 36.99 %, respectively. We believe the inhibition above-mentioned is related to the action of TA, since when performing the REMA test with pure TA (Sigma–Aldrich, Darmstadt, Germany), at the highest concentration of 200 μg mL^{-1}, we detected growth inhibition of *X. citri* (Figure S22, Supporting Information), and obtained an IC_{100} value of 99.93 μg mL^{-1}. However, the MBC results for TA also confirmed that its effect on *X. citri* was only bacteriostatic, even at 200 μg mL^{-1} (Figure S22, Supporting Information).

2.6. G6 Released from Microgels Permeabilize the Membrane and Disrupt Cell Division of *X. citri*

We demonstrated previously that G6 exerts its antibacterial action by multiple mechanisms, which include the permeabilization

of the bacterial membrane and disruption of the cell division apparatus.[19,21,22] However, since G6 was immobilized in the polymeric network of the microgels, it was necessary to verify if the G6-loaded microgels would still retain the same antibacterial properties attributed to the free gallate.

First, we employed the live/dead assay[21] to investigate if the microgels could induce membrane disruption. For that, cells were treated with the microgels and subsequently labeled with the DNA dyes 4′,6-diamidino-2-phenylindol (DAPI) and propidium iodide (PI), which is a combination that enables the identification of viable and unviable cells in a sample. Since PI can only enter the cells with permeabilized membranes, it helps to identify the compounds able to damage membranes. Cells of *X. citri* were exposed for 15 min to the G6-loaded microgels, pVCL/pGMA/BIS/hDerm/G6 and pVCL/pGMA/TA/hDerm/G6, at the concentration equivalent to their IC_{50} values, and we observed that >30 % of the cells were permeabilized to PI (Figure S23, Supporting Information). When the concentrations of the G6-loaded microgels were equivalent to their IC_{100}, >70 % of the *X. citri* cells were PI-permeable after 15 min of contact (Figure S23, Supporting Information). Therefore, the G6-loaded microgels retained the ability to act on the bacterial membrane as the free G6 does. In addition, the G6-loaded microgels exhibited a rather fast activity, where more than half of the cells were affected in the first 15 min of contact. The rapid activity is probably caused by an increased release rate of G6 in saline aqueous solutions, as used for the experiments (Figure S21, Supporting Information).

In order to evaluate if G6 encapsulated into the microgel matrix could still disrupt the bacterial divisional septum, a mutant strain of *X. citri* that is fluorescently labeled for the septum was exposed to G6-loaded microgels and subsequently observed under the microscope. Exposure to the microgels at their IC_{50} for 15 min did not interfere with the bacterial divisional apparatus (Figure S24, Supporting Information). Upon treatment, the divisional septum could still be detected in dividing cells as a fluorescent bar positioned at the center of the rods and perpendicularly oriented with respect to the long axis of the cells. However, by increasing the concentration of the microgels to their IC_{100} led to a complete disappearance of the divisional septa within the same timeframe of 15 min. These results confirmed our previous reports on the activity of G6,[19,21] and, in addition, provided evidence for the proper release of G6 from the microgel matrixes.

2.7. Microgels Protect Citrus Against Bacterial Infection

To assess the ability of microgels to protect citrus plants against *X. citri* infection, nursery trees of C. sinensis cv. Pera, a susceptible host, were spray-covered with microgel dispersions with different degrees of functionalization and subsequently infected with the bacterium. These different degrees of functionalization include the pristine microgel carrier systems, the microgel carrier systems conjugated with anchor peptides and G6-loaded microgel conjugates.

We observed that only the G6-loaded microgels pVCL/pGMA/TA/hDerm/G6 and pVCL/pGMA/BIS/hDerm/G6 were able to protect citrus significantly reducing the number of lesions cm^{-2} produced when compared to the untreated plants (**Figure 6**). This finding correlates with the results of in vitro assays, REMA, and MBC (Figure 5). Untreated plants, sprayed only with saline solution prior to bacterial challenge, exhibited on average 18.22 lesion cm^{-2}, while plants treated with the G6-loaded microgels pVCL/pGMA/BIS/hDerm/G6 and pVCL/pGMA/TA/hDerm/G6 produced 1.90 and 4.55 lesion cm^{-2}, respectively. The G6-loaded microgel pVCL/pGMA/TA/hDerm/G6 was less efficient in protection than pVCL/pGMA/BIS/hDerm/G6 in our experiments. Noteworthy, pVCL/pGMA/BIS/hDerm/G6 reached a protection level comparable to the copper-based commercial product Difere. Plants sprayed with Difere showed on average 1.31 lesion cm^{-2}. In practice, the G6-loaded microgel pVCL/pGMA/BIS/hDerm/G6, when used at 2.75 mg mL^{-1}, performed as well as Difere, and there was no statistic significant difference between them in our analyses. Finally, the remaining microgels without the gallate G6 on their compositions were unable to protect citrus and produced numbers of lesion cm^{-2} statistically similar to the untreated control. The data values corresponding to Figure 6a are listed in Table S2 (Supporting Information).

2.8. Microgel pVCL/pGMA/BIS/hDerm/G6 is Capable of Long-Lasting Protection

Commercial copper-based defensives exhibit the advantage of long-lasting protection due to the fact that they contain metallic copper, which deposits on the plant surfaces, such as leaves, and forms films that can exert a mechanic barrier against pathogens. Subsequently, copper ionic forms produced upon contact with water/moisture can also be killed by microbicidal action. To evaluate if the G6-loaded microgels can also remain on leaves such as metallic copper, and exert long-lasting protection effects, we simulated compound removal by water by introducing a washing step in our plant protection experiments between compound application and bacterial challenge (**Figure 7**). For simplicity, only the G6-loaded microgels that could protect citrus in our previous analyses were considered at the concentration of 2.75 mg mL^{-1}. As a result, it was observed that only pVCL/pGMA/BIS/hDerm/G6 was still effective in protecting citrus leaves against infection by *X. citri*, with an average of 3.98 lesions cm^{-2} (Figure 7). When compared with the experiments without washing, note that the number of lesions cm^{-2} formed doubled; however, the number of lesions cm^{-2} formed is still significantly different from the untreated control, which produced here on average ≈12 lesions cm^{-2}. Plants treated with Difere (commercial copper formulation) showed 0.94 lesion cm^{-2}, which is statically equal to the previous experiment without the washing step. For the plants treated with the G6-loaded microgel pVCL/pGMA/TA/hDerm/G6 leaves had on average 10.48 lesion cm^{-2}, which was statistically equal to the untreated control. This could be due to a more effective fixation to the leaf surface in the case of pVCL/pGMA/BIS/hDerm/G6 microgels, as a more intense fluorescence signal (≈2-fold) could be detected by fluorescence spectroscopy after conjugation of the anchor peptides to the microgel (Figure 3b). The data values corresponding to Figure 7a are listed in Table S3 (Supporting Information).

The copper-based formulation showed a higher foliar fixation capacity than the synthesized microgels, being capable to

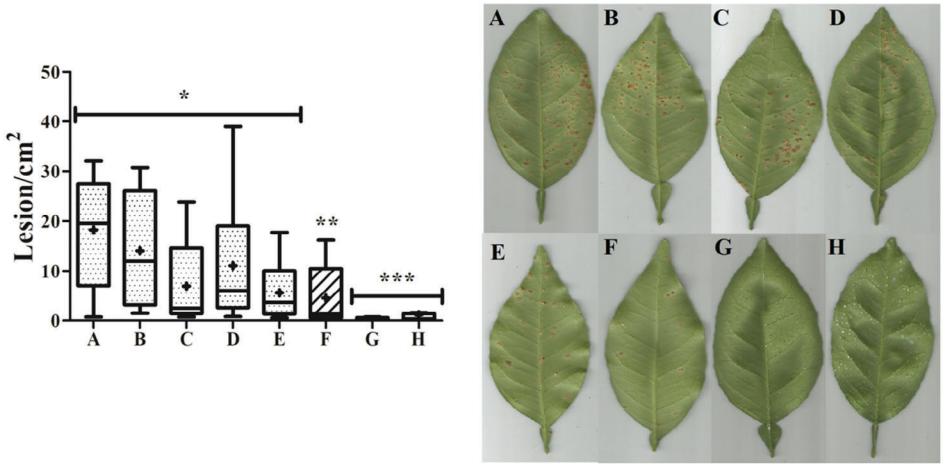

Figure 6. Microgels protect citrus plants against *X. citri* infection. Plants of *C. sinensis* were spray-covered with suspensions of different microgels at 2.75 mg mL^{-1}. 24 h later, plants were challenged with *X. citri*, and after that kept in a greenhouse (average humidity of 77.90 %; average temperature of 26.36 °C) to score for the appearance of citrus canker symptoms. Left panel, boxplot showing the distribution of the numbers of lesion cm^{-2} per leaf documented for all the leaves in a particular treatment, as follows: A) control; B) pVCL/pGMA/BIS; C) pVCL/pGMA/BIS/hDerm; D) pVCL/pGMA/TA; E) pVCL/pGMA/TA/hDerm; F) pVCL/pGMA/TA/hDerm/G6; G) pVCL/pGMA/BIS/hDerm/G6; H) Difere at 2.96 mg mL^{-1} (700 µg mL^{-1} of metallic copper), $N = 12$. The plus signs within the boxes show the mean lesions cm^{-2} of each treatment. The asterisks above the boxes indicate the statistical difference between the treatments based on Kruskal–Wallis Dunn's analysis. Right panel, representative pictures of leaves evaluated in each treatment.

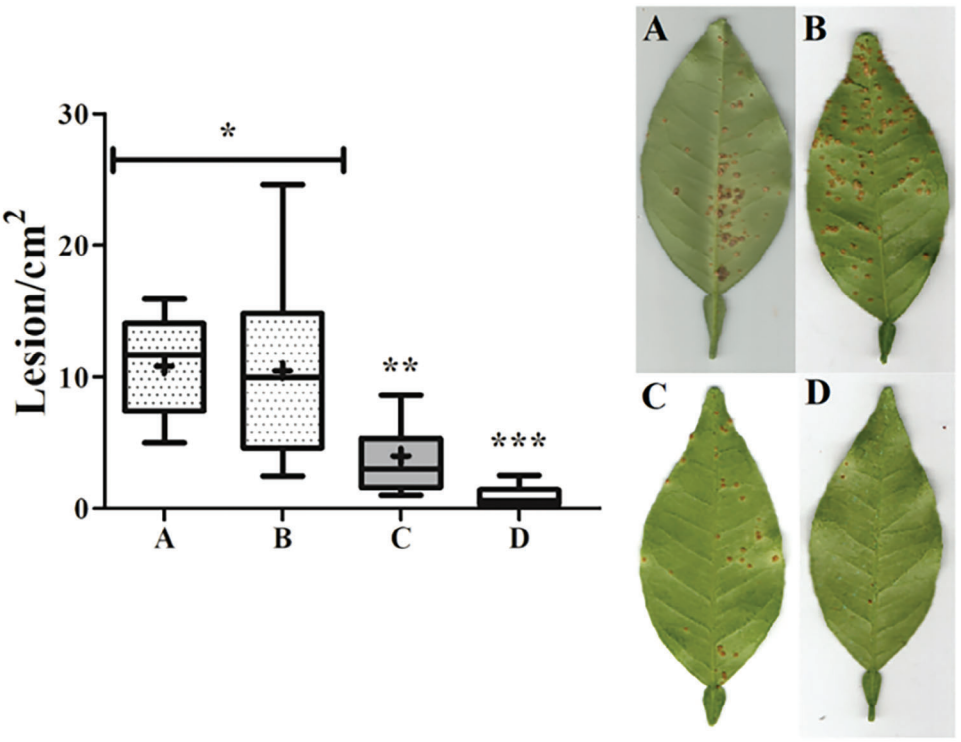

Figure 7. G6-loaded microgels confer residual protection against *X. citri* infection. Rain fastness of the microgels was assessed by introducing a washing step between microgel application and bacterial challenging (average humidity of 77.90 %; average temperature of 26.36 °C). Left panel, boxplot showing the distribution of the numbers of lesions cm^{-2} per leaf documented for all the leaves in a treatment: A) control; B) pVCL/pGMA/TA/hDerm/G6 at 2.75 mg mL^{-1}; C) pVCL/pGMA/BIS/hDerm/G6 at 2.75 mg mL^{-1}; D) Difere at 2.96 mg mL^{-1}, $N = 12$. The plus signs within the boxes show the mean lesions cm^{-2} of each treatment. The asterisks above the boxes indicate the statistical difference between the treatments based on Kruskal–Wallis Dunn's analysis. Right panel, representative pictures of the leaves evaluated per treatment.

maintain its protective effect regardless of the rainfall simulation performed in the experiments. Difere is composed of copper oxychloride, which is the active metallic copper in the product, its non-polarity and insolubility give greater adhesion and resistance to leaching by rain. All microgels synthesized in the present work are dispersible in water.[57,58] On the other hand, the G6-loaded microgel pVCL/pGMA/BIS/hDerm/G6 was the best microgel carrier system synthesized and functionalized, obtaining significant protective action in the greenhouse experiments. Even with a twofold decrease in its protective capacity after the washing step, pVCL/pGMA/BIS/hDerm/G6 displayed a residual effect, showing satisfactory protective results when compared to the untreated and positive controls. In the event of rain, which normally leads to a spreading of the pathogen, the loaded, functional microgels remain at least partially on the leaves and, as suggested by our experimental data, can release G6 to inhibit the spreading of *X. citri*.

3. Conclusion

This work demonstrates the development of a microgel-based plant protection system for citrus plants against the disease citrus canker caused by the bacterial pathogen *Xanthomonas citri*. We aimed to find a more environmentally friendly alternative to the current treatment of citrus canker with highly concentrated and harmful copper formulations.

After synthesis and purification of the microgel carrier systems, a post-functionalization with the anchor peptide eGFP-hDermcidin and a subsequent loading with the biobased, antimicrobial component G6 was performed. It was found that the remarkably high loadings of G6 in microgels can be achieved (up to 40 wt.%). The release of G6 in aqueous media can be modulated by pH and temperature over long time periods (several weeks) suggesting the sustained release and a possibility of long-term protection for plants.

The antimicrobial activities against the Gram-negative pathogen *X. citri* were evaluated using a broad range of different assays. Starting with the combination of REMA and MBC assays, and finally by testing the performance on citrus trees in greenhouse assays including washing steps to obtain the most realistic result in terms of the subsequent application. Both functionalized and loaded microgel systems containing covalent or degradable supramolecular cross-links, are effective in protecting citrus against *X. citri* infection when applied at a minimum concentration of 2.75 mg mL^{-1}. After the washing step, however, only the covalently cross-linked pVCL/pGMA/BIS/hDerm/G6 microgel retained its protective effect against *X. citri*. Therefore, the G6-loaded pVCL/pGMA/BIS/hDerm/G6 microgel stood out as the most promising microgel for field application, presenting protective results against *X. citri* very similar to the commercially available copper formulation Difere.

Furthermore, we believe that microgels as carriers for controlled delivery of active ingredients can be broadly used in agriculture. A key aspect is the low cost of production, even at laboratory scale, but also the safe and straightforward handling of microgel dispersions.[40] Another interesting feature of microgels is their ability to redisperse in aqueous solutions after lyophilization, forming stable colloidal dispersions. Therefore, microgels loaded with active ingredients can be lyophilized to increase their shelf life and reduce the shipping costs. Prior to field application, microgel powders can be redispersed in aqueous solutions and applied to crops using conventional spraying equipment.

4. Experimental Section

Materials: Tannic acid (TA, ACS Reagent, Sigma–Aldrich), 2,2′-azobis(2-methylpropionamidin)-dihydrochloride (V-50, 97 %, Sigma–Aldrich), cetyltrimethylammonium bromide (CTAB, ≥ 99 %, Carl Roth), ultra-pure water (HiPerSolv CHROMANORM, HPLC grade, VWR), dimethyl sulfoxide (DMSO, analytical reagent, with <0.03 % water, VWR), Trizma base (≥ 99.9 %, Sigma), Trizma hydrochloride (≥ 99.0 %, Sigma), dimethyl terephthalate (DMT, ≥ 99 %, standard for quantitative NMR, TraceCERT, Sigma–Aldrich) and DMSO-d_6 (99.8 %, Deutero GmbH) were used as received and without further purification. The two monomers *N*-vinylcaprolactam (VCL, 98 %, Sigma–Aldrich) and glycidyl methacrylate (GMA, ≥ 97 %, Sigma–Aldrich) were distilled *in vacuo* before use. VCL was further purified by recrystallization from *n*-Hexane. All other chemicals used in this study were purchased from Carl Roth GmbH (Karlsruhe, Germany), Sigma-Aldrich Corp. (St. Louis, MO) or AppliChem GmbH (Darmstadt, Germany) and had at least analytical-reagent grade purity. Synthetic genes were obtained from GeneArt AG (Regensburg, Germany). The plasmid pET28a(+) (Novagen, Darmstadt, Germany) was used as expression vector. The *E. coli* strain BL21-Gold (DE3) was purchased from Agilent Technologies (Santa Clara, CA).

Synthesis and Characterization of Hexyl Gallate: The synthesis of hexyl gallate (G6) was achieved by esterification of Fischer reaction between gallic acid and 1-hexanol, under reflux and sulfuric acid catalysis. The crude product was purified over silica gel column chromatography, using hexane, and ethyl acetate (7:3) as mobile phase. The structural identification of G6 was carried out using NMR experiments, including ^{1}H-NMR and ^{13}C-NMR spectroscopy (Figure S12, Supporting Information). Detailed data on synthesis, purification, and identification of G6 had been previously described by the group.[19,22,59]

Synthesis and Characterization of Hexyl Gallate: UV Stability: To investigate the stability of G6 under UV irradiation the antimicrobial compound (≈20 mg) was dissolved in DMSO-d_6 (≈600 µL), transferred to a quartz glass NMR tube, and placed on a horizontal shaker. After 25.62 h of exposure to UV light the sample was measured with ^{1}H-NMR spectroscopy to check for changes in the chemical structure. The UV-LED lamp used was a mounted LED from Thorlabs (M365LP1) and had a wavelength of 365 nm with a bandwidth (FWHM) of 9 nm and an output power of 2 W. The mounted LED was equipped with a collimator adapter (SM2F32-A, Thorlabs) for a wavelength range of 350–700 nm and operated with a T-Cube LED driver (LEDD1B, Thorlabs) with a current of 1.2 A in continuous wave mode.

Synthesis and Characterization of Anchor Peptide: From our laboratory strain collection, five anchor peptides were selected to further test their ability to bind to the orange leaves' surface. The anchor peptides selected are shown in Table S1 (Supporting Information) as well as their proprieties.

The selected anchor peptides were expressed as fusion proteins, having in the N-terminus the indicator protein eGFP in *Escherichia coli* BL21-Gold (DE3), as previously described.[52]

The binding of the peptides on the orange leaves surface was analyzed using confocal microscopy (Leica TCS SP8 microscope, Ex 485 nm, Em 520 nm, argon laser 20% intensity, gain 500, Leica Microsystems GmbH (Wetzlar, Germany)). Young orange leaves were collected from a *Citrus sinensis* tree and washed with water and cut into disks. Cell-free extracts of the eGFP-anchor peptide were used to test the binding (20 µL). After 5 min, the lysate drop was removed, and the disk leaf was washed with TRIS/HCl buffer (pH 8.0, 50 mM) for 5 min. The disks were then analyzed by microscopy.

The selected anchor peptide hDermcidin (hDerm) was expressed as a fusion protein, having, besides the eGFP, a His 6-Tag in the N-terminus, and was purified using a fast protein liquid chromatography (ÄKTAprime, GE Healthcare) with a prepacked ion affinity chromatography column (Ni

Sepharose 6 Fast Flow, GE Healthcare). After purification, samples were desalted using a dialysis membrane (Spectra/Por4, Spectrum Inc., Breda, Netherlands) for further use.

Synthesis and Characterization of Microgels: *Non-degradable Microgels Cross-linked with BIS*: VCL (12.8195 g, 92.101 mmol, 87.4 mol.%) and BIS (0.3249 g, 2.108 mmol, 2 mol.%) were dissolved in deionized water (1000 mL). The solution was stirred (500 rpm) and degassed with nitrogen (60 min). The reaction mixture was then heated to 70 °C. During this time, V-50 (0.1715 g, 0.632 mmol, 0.6 mol.%) was dissolved in deionized water (1 mL). Upon reaching 70 °C, the solution of V-50 was added to the reaction mixture using a syringe. GMA (1.498 g, 1440 µL, 10.538 mmol, 10 mol.%) was added after the initiation (3 min). The polymerization was terminated after 30 min by slowly cooling down to room temperature. The molar percentage was calculated in correlation to the amount of VCL added. For purification of the microgel dispersion, it was dialyzed for at least 3 days against deionized water (5 L) with a cellulose membrane (MWCO 12–14 kDa). The water was exchanged at least twice a day. After purification and lyophilization the yield was determined gravimetrically.

Degradable Microgels Cross-linked with TA: The microgels were synthesized using free radical precipitation polymerization. At first, aqueous stock solutions of TA (0.15 g, 1701.2 g mol^{-1}) dissolved in demineralized water (2 mL) and the surfactant CTAB (0.02 g, 364.46 g mol^{-1}) dissolved in demineralized water (12 mL) were prepared. Then VCL (2 g, 139.2 g mol^{-1}) was dissolved in deionized water (150 mL) in a 250 mL round-bottom flask. After adding CTAB (0.006 g, 3.6 mL) from the stock solution. Subsequently, the solution was degassed with nitrogen for 30 min at room temperature while stirring (500 rpm). After degassing, the reaction mixture was heated to 70 °C. Shortly before reaching the reaction temperature, V-50 (0.05 g, 271.2 g mol^{-1}) was dissolved in demineralized water (1 mL). When the polymerization temperature of 70 °C was reached, the reaction was initiated by adding the V-50 solution with a syringe into the monomer solution. After 3 min the comonomer GMA (217 µL, 0.226 g, 11.1 mol.%, 142.15 g $mol.^{-1}$) was added in one shot using a single-use syringe (1 mL). 15 min after initiation, TA (0.1228 g, 0.5 mol.%) of the TA stock solution was added with a syringe. The molar percentages refer to the used VCL amount. The polymerization was continued for additional 15 min. The polymerization was terminated after 30 min by slowly cooling down to room temperature. To purify the microgel dispersion, it was dialyzed for at least 3 days against deionized water (5 L) with a cellulose membrane (MWCO 12–14 kDa). The water was exchanged at least twice a day. After purification and lyophilization the yield was determined gravimetrically.

Conjugation of Anchor Peptides to Microgels: The microgels, pVCL/pGMA/BIS and pVCL/pGMA/TA were dispersed in a buffer solution (TRIS (50 mM, pH 8)) and stirred at room temperature. A solution of eGFP-hDermcidin (hDerm) was added to the microgel dispersion. The conjugation of the microgels with the anchor peptide was performed overnight (≈18 h). For purification, the microgel conjugates were centrifuged three times (10 min, 12 000 rpm) and redispersed in deionized water.

Investigation of Microgel Anchor Peptide Conjugates: The purified and diluted microgel dispersions (6.7 mg mL^{-1}) were transferred to a black micro titer plate (MTP, PP, flat bottom, 100 µL per well). The fluorescence was measured with a MTP reader FLUOstar Omega MTP Reader using 485 nm excitation and 520 nm emission.

Wax Binding Assay for Microgel Anchor Peptide Conjugates: Wax extraction procedure was performed as described elsewhere[50] with the following modification. For cuticular wax extraction, the orange leaves were immersed in pure chloroform (25 s). For MTP wax coating, the cuticular wax-chloroform mixture was added to each well (60 µg cm^{-2}, 50 µL per well) and the chloroform was completely evaporated (25 °C, 16 h). The purified and diluted microgel dispersions (5 mg mL^{-1}) were transferred to a black 96-well MTP (100 µL per well) and incubated overnight. The next day, the microgel dispersions were discarded and washed briefly with deionized water (200 µL) to remove residual unbound and loosely bound microgels and microgel anchor peptide conjugates. Then the fluorescence was determined with the FLUOstar Omega MTP reader using 485 nm excitation and 520 nm emission. Subsequently, the samples were washed two times with deionized water (200 µL, 25 °C, 5 min, 200 rpm) and the fluorescence was measured each time. To enable a comparison in terms of a relative reduction of bound microgels and microgel anchor-peptide conjugates with the subsequent washing steps, the fluorescence signal of the originally bound material was set to 100 %.

Loading of Microgel/Anchor Peptide Conjugates with Hexyl Gallate: For the loading of conjugated microgels, pVCL/pGMA/BIS/hDerm and pVCL/pGMA/TA/hDerm, with G6, a mass ratio of 1 mg G6 ($3.933 \cdot 10^{-6}$ mol) per 1 mg microgel was used. Microgel/anchor peptide conjugates were stirred at room temperature. G6 was dissolved in DMSO (2.4 wt.% DMSO based on the amount of water volume of the conjugate dispersion) and added to the vigorous stirring dispersion. The stirring of the microgel dispersion was continued overnight (≈18 h). For purification, the loaded microgels were centrifuged three times (20 min, 12 000 rpm) and redispersed in deionized water.

Release of Hexyl Gallates from Microgels: For the release experiments, a dispersion of G6-loaded microgels (15 mL) was dialyzed against deionized water (1.5 L) with the desired pH value (MWCO 12–14 kDa). The release of G6 from the microgels was investigated under different conditions, like temperature (25 and 50 °C) and pH (pH 3, pH 5, pH 7, and pH 9). The samples were subsequently stored at 25 °C (room temperature) or 50 °C for either 6 or 22 days. Additionally, the effect of an isotonic salt concentration (9 g L^{-1}) was investigated at 25 °C and a pH value of 7. Samples (1 mL) of the loaded microgel solutions were taken each day in the first week, then every couple of days. The experiments were running for ≈3 weeks. All samples were freeze-dried and investigated via quantitative ^{1}H-NMR spectroscopy to determine the degree of loading with G6 using the internal standard dimethyl terephthalate (DMT).

Microgel Characterization: *Raman spectroscopy*: Raman spectra were recorded with a Bruker RFS 100/S spectrometer. The samples were stimulated by a Nd:YAG laser with a wavelength of 1064 nm and an output power of 200 mW. Each sample was measured with 1000 scans and covered a spectral range from 400 to 4000 cm^{-1} with a resolution of 4 cm^{-1}. The baseline correction and the analysis of the recorded spectra were carried out with the software OPUS 4.0.

For quantification experiments, pVCL homoloymer chains were homogeneously mixed with TA in different ratios by dissolving in methanol. Subsequently, the methanol evaporated from the mixtures over several days until dry mixtures were obtained and measured.

Dynamic light scattering: The size and size distribution ((polydispersity index (PDI)) of the microgels were characterized by dynamic light scattering (DLS) using a Zetasizer Ultra from the company Malvern Panalytical. Before the measurements, the microgel dispersions (5 µL, 12–15 mg mL^{-1}) were diluted in pure, deionized water (1 mL, HPLC-grade). The diluted dispersion (1 mL) was filled into a single-use plastic cuvette (DTS0012). For every sample, 30 size runs were performed with a duration of 1.68 s. This measurement process was repeated three times. The scattering collection angle was either 90° (side scattering) or 174.7° (back scattering). The temperature-dependent experiments were performed after analog sample preparation in a range from 20 to 60 °C in 2.5 °C steps. The results were evaluated by ZS XPLORER Software.

Electrophoretic light scattering: The surface charge of the microgels was characterized by electrophoretic light scattering (ELS) using a Zetasizer Ultra from the company Malvern Panalytical. Before the measurements, the microgel dispersions (10 µL, 12–15 mg mL^{-1}) were diluted in pure, deionized water (1 mL, HPLC-grade). The diluted dispersion was filled into a cuvette (DTS1070). For every sample, 10 – 30 runs were performed. This measurement process was repeated three times. Between each set of runs, a pause of 10 s was set. The temperature-dependent experiments were performed after analogue sample preparation in a range from 20°C to 60°C in 2.5°C steps. The results were evaluated by ZS XPLORER Software.

Nuclear magnetic resonance spectroscopy: ^{1}H-NMR spectra for G6 quantification were measured with a Bruker DPX-400 FT-NMR spectrometer at a frequency of 400 MHz with a pulse delay of 15 s. For each measurement, 10–15 mg of microgel sample were dissolved in DMSO-d_6 (0.6 mL) containing the internal standard DMT (0.043 mol L^{-1}).

Fluorescence spectroscopy: To determine the signal of microgels functionalized with the anchor peptide hDerm_eGFP a FLUOstar Omega MTP reader (BMG Labtech GmbH, Ortenberg, Germany; excitation (exc.) 485 nm, emission (em.) 520 nm, gain 1000) was used.

Electron microscopy: The microgels morphology in a dry state was investigated by electron microscopy using an ultra-high resolution scanning electron microscope SU9000 from Hitachi-High Technologies America. Samples had been measured in both modes scanning transmission electron mode (STEM) and scanning electron mode (SEM). The samples were prepared by diluting the purified microgel dispersions (10 µL) in deionized water (1000 µL, HPLC grade). Then, the diluted solution (10 µL) was applied on a TEM grid (Carbon Film 200 Mesh Copper Grids, Electron Microscopy Sciences) and dried overnight at room temperature.

Confocal laser scanning microscopy: The fluorescence images were recorded on a Leica SP8 confocal microscope (Leica, Germany). The images were taken with a smart gain of 10%, a pinhole of 1.00, and an Ar laser (λ = 488 nm) with an intensity of 0.5%. The detector PMT2 was used for fluorescent and PMT trans for brightfield images.

Atomic force microscopy: Atomic force microscopy (AFM) was measured with a NanoScope V from Veeco Instruments in tapping mode. ANCH-50 Pointprobe-Silicon SPM-Sensor from Nanoworld with a resonance frequency of 310 kHz and a force constant of 42 N m^{-1} was used as a cantilever. All data were analyzed with the software Gwyddion 2.61.

Antimicrobial Assays: *Microorganisms*: The *Xanthomonas citri* subsp. *citri* used was the isolate 306 (IBSBF 1594). The mutant strain expressing GFP-ZapA, which labels the bacterial septum, was *X. citri amy*::pPM2a-*zapA*.[60] Both bacteria were cultivated at 29 ± 1 °C in solid or liquid NYG medium (5 g L^{-1} peptone, 3 g L^{-1} yeasts extract, and 20 ml L^{-1} glycerol; bacterial agar was added to 15 g L^{-1} for solid medium). Liquid cultures were kept under constant agitation of 200 rpm.

Bacterial growth inhibition assays: The growth inhibitory concentrations (IC) of the microgels against *X. citri* were determined using the resazurin microtiter assay plate method (REMA) with some adaptations.[19] Concentrate solutions of the microgels were prepared by dispersing them in NYG medium to the final concentration of 2.75 mg mL^{-1}. Next, these concentrate solutions were deposited into the wells of a 96-wells microtiter plate (using the first row) and subsequently diluted in a twofold scheme so to give the final concentrations of 1.375, 0.687, 0.343, 0.171, 0.085, 0.042, and 0.021 mg mL^{-1} (rows B-H, respectively). *X. citri* was then inoculated in each well to the final concentration of 10^5 cells. The positive control was kanamycin at 20 µg mL^{-1}, the negative control was the NYG medium without any compound, and the vehicle control was 50 µL of NYG medium and 50 µL of deionized water in order to simulate the wells with the lowest concentration of growth medium. REMA plates were incubated at 29 ± 1 °C for 16 h. To develop the reactions, resazurin (Sigma–Aldrich, Germany) was added to the wells to the final concentration of 0.01 mg mL^{-1}, and plates were further incubated at 29 ± 1 °C for 2 h. NADH produced by live/respiring cells reduces resazurin to fluorescent resorufin, which was detected using the plate reader Synergy H1N1 (BioTek, Winooski, VT, USA) set to excitation and emission wavelengths of 530 and 590 nm, respectively. The data obtained were used to plot the concentration of the microgel versus cell growth inhibition, obtaining the dosage spectrum values. With the dose-response curves a polynomial regression model was applied to determine the percentage of IC_{100} and IC_{50} values (the microgel concentration able to inhibit 100 % and 50 % of *X. citri* in vitro, respectively), as described by Silva et al.[19]

Bactericidal concentration was confirmed with the minimum bactericidal concentration assay (MBC). Before resazurin was added, samples from REMA were transferred to NYG-agar petri dishes with the help of a 96-plate replicator (8 × 12 Sigma–Aldrich, Germany). The plates were then incubated at 29 °C for 48 h to evaluate the ability of the cells to resume growth. These bacterial growth inhibition assays were repeated three times and in triplicates.

Fluorescence microscopy of X. citri cells: The exposure to the microgels was conducted essentially as described for REMA, with some modifications. Cells of *X. citri* were treated with the microgels at their IC_{50} and IC_{100} values for 15 min using 1.5 mL microcentrifuge tubes instead of a 96-wells microtiter plate. The total volume was kept at 100 µL and 10^5 cells per treatment. After the exposure, 900 µL of saline solution (0.86 % NaCl) were added to the tubes in order to dilute the compound and stop the reaction. Cells were stained with propidium iodide (PI) at 10 µg mL^{-1} and 4′,6-diamidino-2-phenylin-dole (DAPI) at 20 mg mL^{-1}. DAPI stains all cells, while PI penetrates only cells with damaged cytoplasmatic membranes. Untreated cells were used as negative control, and the positive control for membrane disruption were cells subjected to thermal stress.[59]

To assess if the microgels could interfere with the bacterial divisome, the *X. citri* mutant expressing GFP-ZapA was exposed to the microgels exactly as described above. Following exposure, cells were precipitated by centrifugation at 4000 ×*g* for 5 min, the supernatant was discarded, and the cells mass was dissolved in 100 µL of saline solution (0.86 % NaCl).

All the cell samples were immobilized onto agarose-covered slides and immediately observed under a BX-61 microscope (Olympus; Tokyo, Japan), equipped with a monochromatic camera OrcaFlash 2.8 (Hamamatsu, Japan). Images were captured and processed with the help of the software CellSens Dimension (Olympus). Experiments were conducted three times and in triplicates (at least 100 individuals (n = 100) were evaluated per treatment for quantification purposes).

Greenhouse assays: The ability of the microgels to protect against *X. citri* infection was evaluated using nursery trees of the susceptible host *Citrus sinensis* cultivar Pera. Plants of ≈50 cm tall were purchased from Citrograf (https://www.citrograf.com.br) and kept in a greenhouse with controlled humidity and temperature (average humidity of 77.90 % with a maximum of 92.70 % and a minimum of 50.27 %; average temperature of 26.36 °C, with a maximum of 37.54 °C and a minimum of 17.84 °C, during all the experiment period from 06/11/2020 to 22/01/2021), and automated fertigation. For the treatments, flushes containing leaves of ≈5 cm were sprayed with the microgel dispersions in a concentration of 2.75 mg mL^{-1} until the run-off point (this was the highest concentration tested in the REMA and MBC assays). After 24 h, the plants were spray-covered with a *X. citri* suspension prepared in saline solution (0.86 % NaCl) containing 10^8 CFU mL^{-1}. For the positive control of protection, plants were sprayed with the commercial copper formulation Difere (35 % w/v metallic copper) at the recommended concentration of 2.96 mg mL^{-1} (700 µg mL^{-1} of metallic copper; Oxiquímica Agrociência Ltda. Jaboticabal, Brazil), and the negative control for protection was saline solution (0.86 % NaCl). After the inoculation step, plants were covered with transparent plastic bags for 24 h to help infection. Plants were monitored over the course of 35 days for the appearance of citrus canker symptoms. The experiment was performed with two plants per group of treatment, with one marked branch per plant. At the end of the experiments, leaves were detached and digitalized at 600 DPI. The software ImageJ (Fiji) was used to evaluate bacterial infection and infection severity, which were expressed as the number of citrus canker lesions formed per leaf area.[22] The data obtained were submitted to non-parametrical statistical analysis of Kruskal-Wallis (Dunn), with three degrees of freedom using the software BioEstat 4.

To evaluate the rain fastness of the microgels, a washing step was introduced between microgel application and bacterial infection. The experimental procedure described above was essentially the same, however, before the bacterial inoculation step, plants were sprayed with saline solution (0.86 % NaCl) until the run-off point. Data acquisition and analyses were identical as above.

Supporting Information

Supporting Information is available from the Wiley Online Library or from the author.

Acknowledgements

S.B., G.D., and L.C.d.L.N. contributed equally to this work. S.B. would like to express her gratitude toward Yannick J. Nußbaum and Sven Pudleiner

for their help as research students as well as Jan Grotelüschen for his assistance as a student helper and Jan Luca Clemens and Jan Niklas Zinn for their support as trainees. The authors wish to thank Silke Boinski and Stefan Hauk for the microscopy measurements of our microgel samples. The authors acknowledge the measurements of Raman spectroscopy and thank Bea Becker. Further the authors appreciate the extraction of wax from orange tree leaves by Christin Wittmann as well as the help and advice of Kevin Broi with the setup to investigate UV stability of G6. G.D. received a Ph.D. scholarship from Fundação de amparo à pesquisa do estado de São Paulo (FAPESP 2017/07306-9 and FAPESP 2018/23306-1). A.P. thanks the Deutsche Forschungsgemeinschaft (DFG) for financial support within the Collaborative Research Center SFB 985 (grant no. 191948804). Parts of the analytical investigations were performed at the Center for Chemical Polymer Technology CPT, which was supported by the European Commission and the federal state of North Rhine-Westphalia (grant no. 300088302). Financial support is acknowledged from BMBF (grant no. 031B0384), FAPESP (grant no. 2015/50162-2), INCT Citros (FAPESP: grant no. 2014/50880-0 and CNPq: grant no. 465 440/2014-2), NWO (grant no. 21.401) and Leibniz Competition - Leibniz Transfer (grant no. T130/2022).

Open access funding enabled and organized by Projekt DEAL.

Conflict of Interest

The authors declare no conflict of interest.

Data Availability Statement

The data that support the findings of this study are available from the corresponding author upon reasonable request.

Keywords

alkyl gallates, anchor peptides, citrus canker, drug delivery, microgels, plant protection, tannic acid

Received: May 21, 2023
Revised: October 25, 2023
Published online: November 8, 2023

[1] A. Duarte, J. Fernandes, J. Bernardes, G. Miguel, *J. Spat. Organ. Dyn.* **2016**, *IV*, 289.
[2] FAOSTAT-Food and Agriculture Organization of the United Nations, https://www.nationmaster.com/nmx/ranking/citrus-production (accessed: September **2021**).
[3] M. T. Ireno, V. C. Silva, J. A. Silva, A. B. Convento, L. Paulo, S. Euzebio, L. Bermejo, *Rev. Científica Eletrônica Agron.* **2014**, *25*, 34.
[4] M. F. Neves, V. G. Trombin, P. Milan, F. F. Lopes, F. Cressoni, R. Kalaki, *O Retrato da Citricultura Brasileira, CitrusBR, Ribeirão Preto*, Sao Paulo, Brazil, https://citrusbr.com/wp-content/uploads/2020/10/Retrato_Citricultura_Brasileira_MarcosFava.pdf (accessed: October 2023).
[5] A. A. Vojnov, A. Morais Do Amaral, J. M. Dow, A. P. Castagnaro, M. R. Marano, *Appl. Microbiol. Biotechnol.* **2010**, *87*, 467.
[6] L. Mendonça, L. Zambolim, J. Badel, *J. Bacteriol. Mycol.* **2017**, *5*, 340.
[7] T. R. Gottwald, J. H. Graham, T. S. Schubert, *Plant Heal. Prog.* **2002**, *3*, 15.
[8] C. H. Bock, J. H. Graham, T. R. Gottwald, A. Z. Cook, P. E. Parker, *Plant Dis* **2010**, *94*, 725.
[9] F. Behlau, *Trop. Plant Pathol.* **2021**, *46*, 1.
[10] M. Zhang, Q. Meng, *Pattern Recognit. Lett.* **2011**, *32*, 2036.
[11] C. M. Ference, A. M. Gochez, F. Behlau, N. Wang, J. H. Graham, J. B. Jones, *Mol. Plant Pathol.* **2018**, *19*, 1302.
[12] C. F. C. Zamuner, G. Dilarri, L. C. Bonci, L. L. Saldanha, F. Behlau, T. G. S. Marin, D. C. Sass, M. Bacci, H. Ferreira, *Trop. Plant Pathol.* **2020**, *45*, 701.
[13] J. R. Lamichhane, E. Osdaghi, F. Behlau, J. Köhl, J. B. Jones, J. N. Aubertot, *Agron. Sustainable Dev.* **2018**, *38*, 28.
[14] F. C. Coelho, R. Squitti, M. Ventriglia, G. Cerchiaro, J. P. Daher, J. G. Rocha, M. C. A. Rongioletti, A.-C. Moonen, *Biomolecules* **2020**, *10*, 897.
[15] D. Fernández-Calviño, J. C. Nóvoa-Muñoz, M. Díaz-Raviña, M. Arias-Estévez, *Geoderma* **2009**, *153*, 119.
[16] G. Tóth, T. Hermann, M. R. Da Silva, L. Montanarella, *Environ. Int.* **2016**, *88*, 299.
[17] IFOAM, Report of the copper application in organic agriculture in Europe, https://www.ifoam-eu.org/sites/default/files/ifoam_eu_copper_minimisation_in_organic_farming_may2018_0.pdf (accessed: January **2020**).
[18] F. Behlau, B. I. Canteros, G. V. Minsavage, J. B. Jones, J. H. Graham, *Appl. Environ. Microbiol.* **2011**, *77*, 4089.
[19] I. C. Silva, L. O. Regasini, M. S. Petrônio, D. H. S. Silva, V. S. Bolzani, J. Belasque, L. V. S. Sacramento, H. Ferreira, *J. Bacteriol.* **2013**, *195*, 85.
[20] I. Silva, H. Ferreira, *Bio-Protocol* **2013**, *3*, e861.
[21] E. Król, A. De Sousa Borges, I. Da Silva, C. R. Polaquini, L. O. Regasini, H. Ferreira, D.-J. Scheffers, *Front. Microbiol.* **2015**, *6*, 1313.
[22] L. B. Cavalca, C. F. C. Zamuner, L. L. Saldanha, C. R. Polaquini, L. O. Regasini, F. Behlau, H. Ferreira, *Microbiologyopen* **2020**, *9*, e1104.
[23] A. Fernandez-Nieves, H. M. Wyss, J. Mattsson, D. A. Weitz, *Microgel Suspensions: Fundamentals and Applications*, Wiley-VCH Verlag GmbH & Co. KGaA, Weinheim, Germany **2011**.
[24] A. Pich, W. Richtering, *Chemical Design of Responsive Microgels, Advances i.*, Springer, Berlin, Germany **2010**.
[25] F. A. Plamper, W. Richtering, *Acc. Chem. Res.* **2017**, *50*, 131.
[26] M. Karg, A. Pich, T. Hellweg, T. Hoare, L. A. Lyon, J. J. Crassous, D. Suzuki, R. A. Gumerov, S. Schneider, I. I. Potemkin, W. Richtering, *Langmuir* **2019**, *35*, 6231.
[27] K. Kratz, T. Hellweg, W. Eimer, *Polymer* **2001**, *42*, 6631.
[28] H. Dalmont, O. Pinprayoon, B. R. Saunders, *Langmuir* **2008**, *24*, 2834.
[29] Q. M. Zhang, W. Wang, Y.-Q. Su, E. J. M. Hensen, M. J. Serpe, *Chem. Mater.* **2016**, *28*, 259.
[30] M. J. Bergman, J. S. Pedersen, P. Schurtenberger, N. Boon, *Soft Matter* **2020**, *16*, 2786.
[31] T. Kharandiuk, K. H. Tan, W. Xu, F. Weitenhagen, S. Braun, R. Göstl, A. Pich, *Chem. Sci.* **2022**, *13*, 11304.
[32] M. F. Schulte, E. Izak-Nau, S. Braun, A. Pich, W. Richtering, R. Göstl, *Chem. Soc. Rev.* **2022**, *51*, 2939.
[33] W. Xu, A. A. Rudov, R. Schroeder, I. V. Portnov, W. Richtering, I. I. Potemkin, A. Pich, *Biomacromolecules* **2019**, *20*, 1578.
[34] X. Wenjing, R. Andrey, O. Alex, W. Sarah, K. Michael, S. Ricarda, R. Walter, P. I. I. Potemkin, W. Dominik, P. Andrij, *Angew. Chem.* **2020**, *132*, 1264.
[35] T. Belthle, D. E. Demco, A. Pich, *Macromolecules* **2022**, *53*, 844.
[36] T. Belthle, A. Pich, *Mol. Syst. Des. Eng.* **2022**, *7*, 1207.
[37] X. Li, H. Sun, H. Li, C. Hu, Y.u Luo, X. Shi, A. Pich, *Adv. Funct. Mater.* **2021**, *31*, 2100227.
[38] E. Gau, D. M. Mate, Z. Zou, A. Oppermann, A. Töpel, F. Jakob, D. Wöll, U. Schwaneberg, A. Pich, *Biomacromolecules* **2017**, *18*, 2789.
[39] S.-H. Jung, S. Bulut, L. P. B. Busca Guerzoni, D. Günther, S. Braun, L. De Laporte, A. Pich, *J. Colloid Interface Sci.* **2022**, *617*, 409.
[40] R. A. Meurer, S. Kemper, S. Knopp, T. Eichert, F. Jakob, H. E. Goldbach, U. Schwaneberg, A. Pich, *Angew. Chemie., Int. Ed.* **2017**, *56*, 7380.

[41] L. Apitius, S. Buschmann, C. Bergs, D. Schönauer, F. Jakob, A. Pich, U. Schwaneberg, *Macromol. Biosci.* **2019**, *19*, 190025.
[42] S. Dedisch, A. Wiens, M. D. Davari, D. Söder, C. Rodriguez-Emmenegger, F. Jakob, U. Schwaneberg, *Biotechnol. Bioeng.* **2020**, *117*, 49.
[43] Y. Gueguen, R. Bernard, F. Julie, S. Paulina, D.-G. Delphine, V. Franck, B. Philippe, B. Evelyne, *Mol. Immunol.* **2009**, *46*, 516.
[44] M. Duperthuy, J. Binesse, F. Le Roux, B. Romestand, A. Caro, P. Got, A. Givaudan, D. Mazel, E. Bachère, D. Destoumieux-Garzón, *Environ. Microbiol.* **2010**, *12*, 951.
[45] S. Kalogiannidis, D. Kalfas, F. Chatzitheodoridis, O. Papaevangelou, *Land* **2022**, *11*, 1680.
[46] M. Saubin, C. Louet, L. Bousset, F. Fabre, P. Frey, I. Fudal, F. Grognard, F. Hamelin, L. Mailleret, S. Stoeckel, S. Touzeau, B. Petre, F. Halkett, *Mol. Ecol.* **2023**, *32*, 2461.
[47] T. C. Sparks, R. J. Bryant, *Pest Manag. Sci.* **2022**, *78*, 399.
[48] D. Schiavi, S. Francesconi, A. R. Taddei, E. Fortunati, G. M. Balestra, *Sci. Rep.* **2022**, *12*, 6149.
[49] L. Hussmann, T. Belthle, D. E. Demco, R. Fechete, A. Pich, *Soft Matter* **2021**, *17*, 8678.
[50] J. Dittrich, C. Brethauer, L. Goncharenko, J. Bührmann, V. Zeisler-Diehl, S. Pariyar, F. Jakob, T. Kurkina, L. Schreiber, U. Schwaneberg, H. Gohlke, *ACS Appl. Mater. Interfaces* **2022**, *14*, 28412.
[51] M. Nöth, Z. Zou, I. El-Awaad, L. C. De Lencastre Novaes, G. Dilarri, M. D. Davari, H. Ferreira, F. Jakob, U. Schwaneberg, *Biotechnol. Bioeng.* **2021**, *118*, 1520.
[52] K. Rübsam, B. Stomps, A. Böker, F. Jakob, U. Schwaneberg, *Polymer* **2017**, *116*, 124.
[53] Y. Ji, Y. Lu, H. Puetz, U. Schwaneberg, *Methods Enzymol* **2021**, *648*, 271.
[54] M. Cipriano-Salazar, S. Rojas-Hernández, J. Olivares-Pérez, R. Jiménez-Guillén, B. Cruz-Lagunas, L. M. Camacho-Díaz, A. E. Ugbogu, *Microb. Pathog.* **2018**, *117*, 255.
[55] G. Dong, H. Liu, X. Yu, X. Zhang, H. Lu, T. Zhou, J. Cao, *Nat. Prod. Res.* **2018**, *32*, 2225.
[56] C. Zhu, M. Lei, M. Andargie, J. Zeng, J. Li, *Physiol. Mol. Plant Pathol.* **2019**, *107*, 46.
[57] C. M. López, A. Pich, *Macromol. Rapid Commun.* **2018**, *39*, 1700808.
[58] C. Molano-López, S. Braun, M. Kather, A. Töpel, G. van Wissen, A. Pich, *Macromol. Chem. Phys.* **2023**, *224*, 2200213.
[59] A. Savietto, C. R. Polaquini, M. Kopacz, D.-J. Scheffers, B. C. Marques, L. O. Regasini, H. Ferreira, *Arch. Microbiol.* **2018**, *200*, 929.
[60] P. M. M. Martins, I. F. Lau, M. Bacci, J. Belasque, A. M. Do Amaral, S. R. Taboga, H. Ferreira, *FEMS Microbiol. Lett.* **2010**, *310*, 76.